Inviscid Drag Prediction for Transonic Transport Wings Using a Full-Potential Method

J. van der Vooren* and A. J. van der Wees†
National Aerospace Laboratory, Amsterdam, The Netherlands

A theory of drag analysis in full-potential flow, based on generalization and extension of Garabedian's and McFadden's idea of determining wave drag by volume integration of the artificial viscosity, is summarized. The applicability of the theory is restricted to shock-capturing numerical methods (such as, e.g., finite-volume methods), where artificial viscosity is essential for proper performance. Two mesh refinement experiments on nested grids have been carried out for the DFVLR-F4-wing in transonic flow, using CH- as well as CO-topology grids. The MATRICS code used in the experiments is first-order accurate in the mesh size throughout supersonic flow regions. It is concluded that CO-topology grids are better suited for drag analysis than are CH-topology grids. It is also concluded that the accuracy of each individual drag component can be improved by extrapolating to the limit of vanishing mesh size. Finally, to avoid excessively fine grids in an engineering environment, the need is stressed for artificial viscosity terms that are second-order small in the mesh size in supersonic flow regions, except for the immediate vicinity of the shock waves. However, extrapolations procedures are believed to remain necessary for accurate drag prediction.

I. Introduction

At the Symposium Transsonicum III in Göttingen, Germany, May 1988, it was observed by Rubbert of Boeing that viscous/inviscid full-potential interaction methods are adequate for the design condition of transonic transport aircraft from the practical point of view. An important background of this observation is no doubt the urge for quick turnaround times in the design process. Today, Euler methods require yet substantially more computational time. Also, full-potential methods have been more widely used in inverse design calculations. Reliable application of full-potential methods in transonic transport wing design requires ultimately, however, that these methods are coupled with a boundary-layer method (e.g., Ref. 2). In such cases, full-potential methods employing fully conservative or pseudo Rankine-Hugoniot type of shock capture are mandatory for reliable prediction of the flow.

At the National Aerospace Laboratory (NLR), research is in progress on the reliable prediction of drag and its components—induced drag, wave drag, and boundary-layer drag—for transport wings under transonic cruise conditions using the in-house-developed full-potential code MATRICS.[3] MATRICS is based on a finite-volume scheme and utilizes a multigrid solver employing incomplete lower upper decomposition/strongly implicit procedure (ILU/SIP) smoothing for rapid, robust convergence and high convergence levels.[4]

At present, MATRICS can handle wing-alone and wing/body configurations on CH- and CO-topology grids and is operational on the NEC SX-2 supercomputer at NLR, allowing grids of up to about 550.000 grid points, running in core. Options for fully conservative as well as nonconservative shock capture are available. The extension of MATRICS to take into account viscous effects through coupling with a boundary-layer solver has been initiated (MATRICS-V project).

In MATRICS, which is first-order accurate in the mesh size in supersonic regions of the flow, the spurious contribution in the drag balance that arises from the production of spurious momentum in supersonic accelerating parts of the flowfield is of the order of the mesh size. This implies that this spurious drag component must halve upon mesh halving, provided that the mesh size is sufficiently small. For transonic flow, this property has suggested the possibility of using linear extrapolation to zero mesh size for the accurate determination of the wave drag and also the induced drag and the static pressure drag. Systematic mesh refinement experiments will be discussed in an attempt to substantiate this procedure.

II. Overview of Flow Equations

MATRICS is based on a fully conservative finite-volume scheme for the full-potential equation in strong conservation form. The scheme is second-order accurate in the mesh size in subsonic parts of the flow and first-order accurate in supersonic parts of the flow. For the capture of supersonic/subsonic shock waves, a Godunov-type shock operator is used. The modified equation of the scheme is

$$(\rho u + P)_x + (\rho v + Q)_y + (\rho w + R)_z = 0 \tag{1}$$

Here, the density ρ is

$$\rho = \{1 + [(\gamma - 1)/2]\, M_\infty^2\, (1 - q^2)\}^{1/(\gamma - 1)} \tag{2}$$

with

$$q^2 = u^2 + v^2 + w^2 \tag{3}$$

The velocity components u, v, and w derive from the velocity potential φ as follows:

$$u = \varphi_x, \qquad v = \varphi_y, \qquad w = \varphi_z \tag{4}$$

Artificial viscosity is introduced through the artificial viscous fluxes P, Q, and R, which are of the order of the mesh size in supersonic parts of the flow,

$$P = -\epsilon_x \text{ sign } [u](u/q)\rho(1 - M^2)q_x\, \Delta_x \tag{5a}$$

$$Q = -\epsilon_y \text{ sign } [v](v/q)\rho(1 - M^2)q_y\, \Delta_y \tag{5b}$$

Presented as Paper 90-0576 at the AIAA 28th Aerospace Sciences Meeting, Reno, NV, Jan. 8–11, 1990; received May 12, 1990; revision received March 30, 1991; accepted for publication April 17, 1991.

*Senior Research Scientist, Mathematical Models and Methods Department, Informatics Division, P.O. Box 90502, 1006 BM.

†Research Scientist, Numerical Mathematics and Applications Programming Department, Informatics Division, P.O. Box 90502, 1006 BM.

$$R = -\epsilon_z \text{ sign } [w](w/q)\rho(1-M^2)q_z\,\Delta_z \tag{5c}$$

Here ϵ_x, ϵ_y, and ϵ_z are positive and of order $\mathcal{O}[1]$ in supersonic flow parts and zero in subsonic flow parts.

The finite-volume discretization of Eq. (1) can be described in terms of discrete operators for the different situations of subsonic, supersonic, and sonic flow, and of supersonic/subsonic shock waves. In particular, the shock operators for the supersonic/subsonic shock waves guarantee the conservation of mass across such shock waves if the fully conservative option in MATRICS is used.

Away from shock waves, the modified full-potential equation (1) can be written in the alternative form

$$(\rho u)_x + (\rho v)_y + (\rho w)_z = m \tag{6}$$

where

$$m = -(P_x + Q_y + R_z) \tag{7}$$

can be interpreted as a distributed mass source per unit volume.

Then the corresponding x-momentum equation is

$$(\rho u^2 + p)_x + (\rho v u)_y + (\rho w u)_z = mu \tag{8}$$

where p is the static pressure and the x direction is the freestream direction.

The effect of artificial viscosity, which is here of first order in the mesh size, is in general to smear out shock waves (true discontinuities in the flow) to narrow zones of steep gradients. However, the artificial viscosity in potential codes and also in MATRICS is only nonzero in supersonic parts of the flow. Then, only supersonic/supersonic shock waves smear out completely. Supersonic/subsonic shock waves smear out only for the supersonic to sonic part and reduce, in fact, to a narrow zone of steep gradients with sonic conditions on its downstream side, immediately followed by a (captured) true discontinuity with sonic conditions on its upstream side (Fig. 1). This discontinuity is, of course, considerably weaker than the full shock wave and will be referred to as the "shock remainder."

III. Drag Analysis

Based on the x-momentum equation (8), the following expression for the pressure drag Dp can be derived if the fully conservative option in MATRICS is used.[5]

$$\begin{aligned} Dp = &-\int_{S_T}[(p-p_\infty)+\rho(u-u_\infty)u]\,dS \\ &+\int_{S_S}[(p_d-\overset{*}{p}_u)n_x+\rho_d q_{nd}(u_d-\overset{*}{u}_u)]\,dS \\ &+\int_{V_{M>1}}(\bar{P}u_x+\bar{Q}u_y+\bar{R}u_z)\,dV \end{aligned} \tag{9}$$

Here S_T is the so-called Trefftz plane, S_S are the upstream surfaces of the shock remainders of the supersonic/subsonic shock waves, and $V_{M>1}$ are the supersonic enclosures in the flow. The suffices u and d refer to the upstream and downstream side of the shock remainder surfaces, n is the downstream pointing unit normal vector on these surfaces, the asterisk refers to sonic conditions, and

$$q_n = un_x + vn_y + wn_z \tag{10}$$

is the velocity normal to the shock remainder surfaces.

Finally, $\bar{P}$, $\bar{Q}$, and $\bar{R}$ are reference artificial viscous fluxes satisfying the requirement

$$\bar{P} \sim \frac{u}{q}, \qquad Q \sim \frac{v}{q}, \qquad \bar{R} \sim \frac{w}{q} \tag{11}$$

Such artificial viscous fluxes can be generated by retarding the mass flux ρq in supersonic enclosures precisely against the flow direction.

Assuming small disturbances in the Trefftz plane, the first integral in Eq. (9) can be expanded as follows:

$$\begin{aligned} &-\int_{S_T}[(p-p_\infty)+\rho(u-u_\infty)u]\,dS \\ &=\frac{1}{2}\rho_\infty\int_{S_T}(v^2+w^2)\,dS+0\left[\left(\frac{v^2+w^2}{u_\infty^2}\right)^2\right] \end{aligned} \tag{12}$$

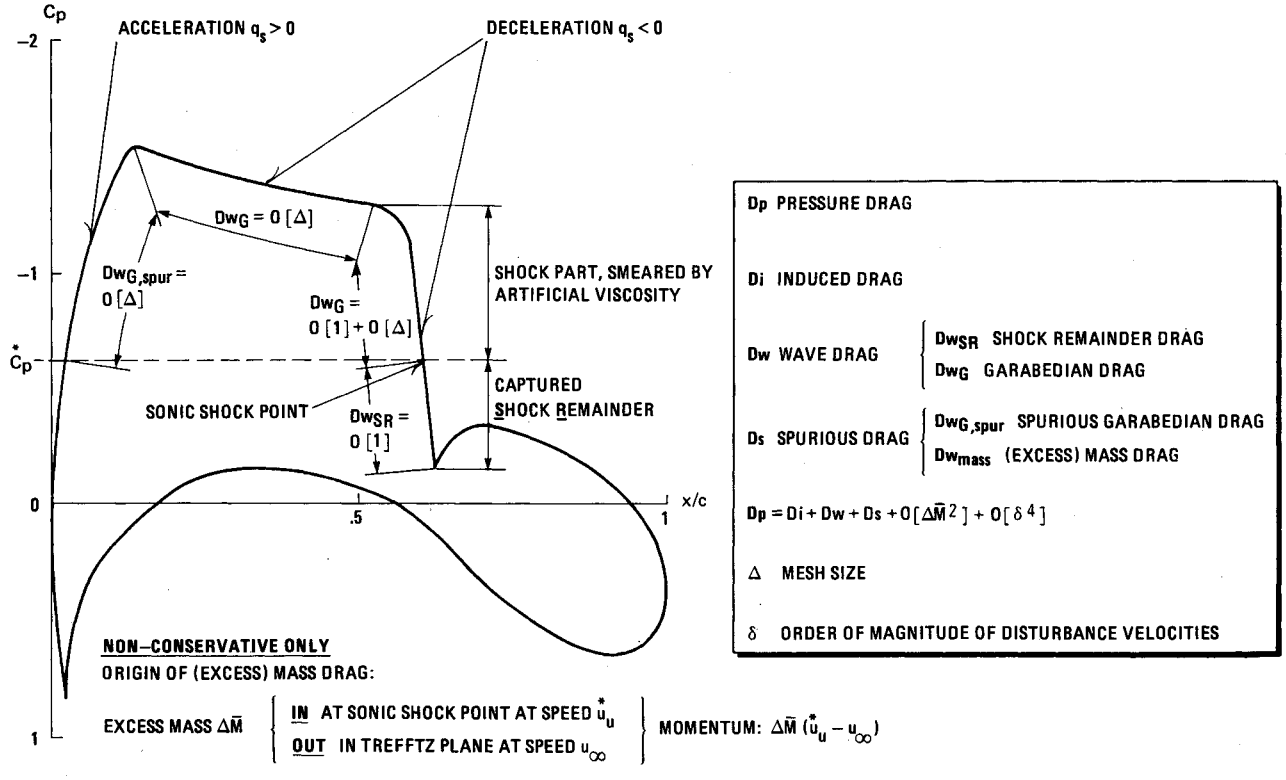

Fig. 1 Pressure distribution on wing section showing the origin of wave drag components and the drag balance.

Here the first integral on the right side is the induced drag Di as calculated from Trefftz-plane integration,

$$Di = \tfrac{1}{2}\rho_\infty \int_{S_T} (v^2 + w^2)\, dS \tag{13}$$

The third integral in Eq. (9) is the generalization[5] of Garabedian's and McFadden's idea of determining wave drag by volume integration of the artificial viscosity[6-8] and is precisely the x momentum that is being produced in supersonic enclosures as a consequence of artificial viscosity. As momentum production is the wave drag mechanism in potential flow, this integral obviously contributes to the wave drag Dw. However, since a smeared-out shock wave is always in decelerating flow, all contributions in the integral stemming from accelerating supersonic flow are of spurious character and must be disregarded. This observation has already been made before by Garabedian[6] and Garabedian and McFadden.[7,8] Consequently, the integral is split into two terms (Fig. 1), viz., the Garabedian (wave) drag

$$Dw_G = \int_{V_{M>1, q_s<0}} (\bar{P}u_x + \bar{Q}u_y + \bar{R}u_z)\, dV \tag{14}$$

and the spurious Garabedian (wave) drag

$$Dw_{G,\text{spur}} = \int_{V_{M>1, q_s>0}} (\bar{P}u_x + \bar{Q}u_y + \bar{R}u_z)\, dV \tag{15}$$

Here s is the (local) streamwise coordinate and q_s the (local) acceleration.

The second integral in Eq. (9) is an extension[5] of Garabedian's[6] and Garabedian's and McFadden's[7,8] ideas and represents the x-momentum production of the shock remainders of the supersonic/subsonic shock waves. Consequently, the integral will be referred to as the shock remainder (wave) drag (Fig. 1),

$$Dw_{SR} = \int_{S_S} [(p_d - \overset{*}{p}_u)n_x + \rho_d q_{nd}(u_d - \overset{*}{u}_u)]\, dS \tag{16}$$

This wave drag component, which has not been considered by Garabedian[6] or Garabedian and McFadden,[7,8] nor by Ross,[9] is in fact the main source of differences in wave drag as it should be obtained from fully conservative and nonconservative full-potential codes (compare with Ref. 5).

In view of the preceding analysis, there holds the following theoretical drag balance:

$$Dp = Di + Dw + Ds + 0\left[\left(\frac{v^2 + w^2}{u_\infty^2}\right)^2\right] \tag{17}$$

where the wave drag Dw and the spurious drag Ds are respectively defined by (Fig. 1)

$$Dw = Dw_G + Dw_{SR} \tag{18}$$

and by

$$Ds = Dw_{G,\text{spur}} \tag{19}$$

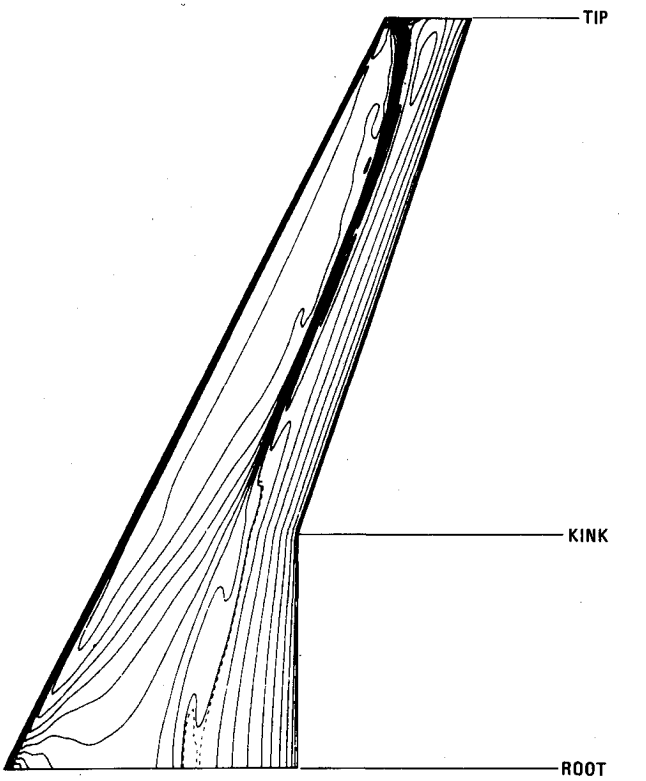

Fig. 2 Planform of the DFVLR-F4-wing and upper surface isobars for the transonic condition $M_\infty = 0.75$, $\alpha = 0.84$ deg.

Details on how the previously defined drag components are implemented, and in particular on how the reference artificial viscosity is determined from the actual artificial viscosity in MATRICS, are given in Ref. 5.

Test calculations for the almost exactly two-dimensional flow at the midspan section of a simple nonswept wing have inspired confidence in the results of the described drag analysis.[1]

IV. Mesh Refinement Experiments

Two mesh refinement experiments have been carried out on CH- as well as on CO-topology grids using the fully conservative MATRICS option for the DFVLR-F4-wing in the transonic case $M_\infty = 0.75$, $\alpha = 0.84$ deg (Fig. 2). Calculations were carried out on the NEC SX-2 supercomputer at NLR in 32 bits precision, using grids of up to about 550.000 grid points. Each run was converged to the point where all drag components could be considered having reached their end value. This required a reduction of the mean and maximum residual by three orders of magnitude. Note that a reduction of two orders of magnitude is already sufficient for a reliable pressure distribution and a proper lift value.

Table 1 Survey of grids used in the mesh refinement experiments for CH- and CO-topology grids

Sequence	Grid generator	Number of meshes: Streamwise Total	Streamwise On wing	Spanwise Total	Spanwise On wing	Wing—normal	No. of cells
CH	MATGRID	80	48	16	9	16	20,480
		120	72	24	15	24	69,120
		160	96	32	19	32	163,840
		240	144	48	31	48	552,960
CO	MATGRID	80	48	16	12	16	20,480
		120	72	24	18	24	69,120
		160	96	32	24	32	163,840
		240	144	48	36	48	552,960

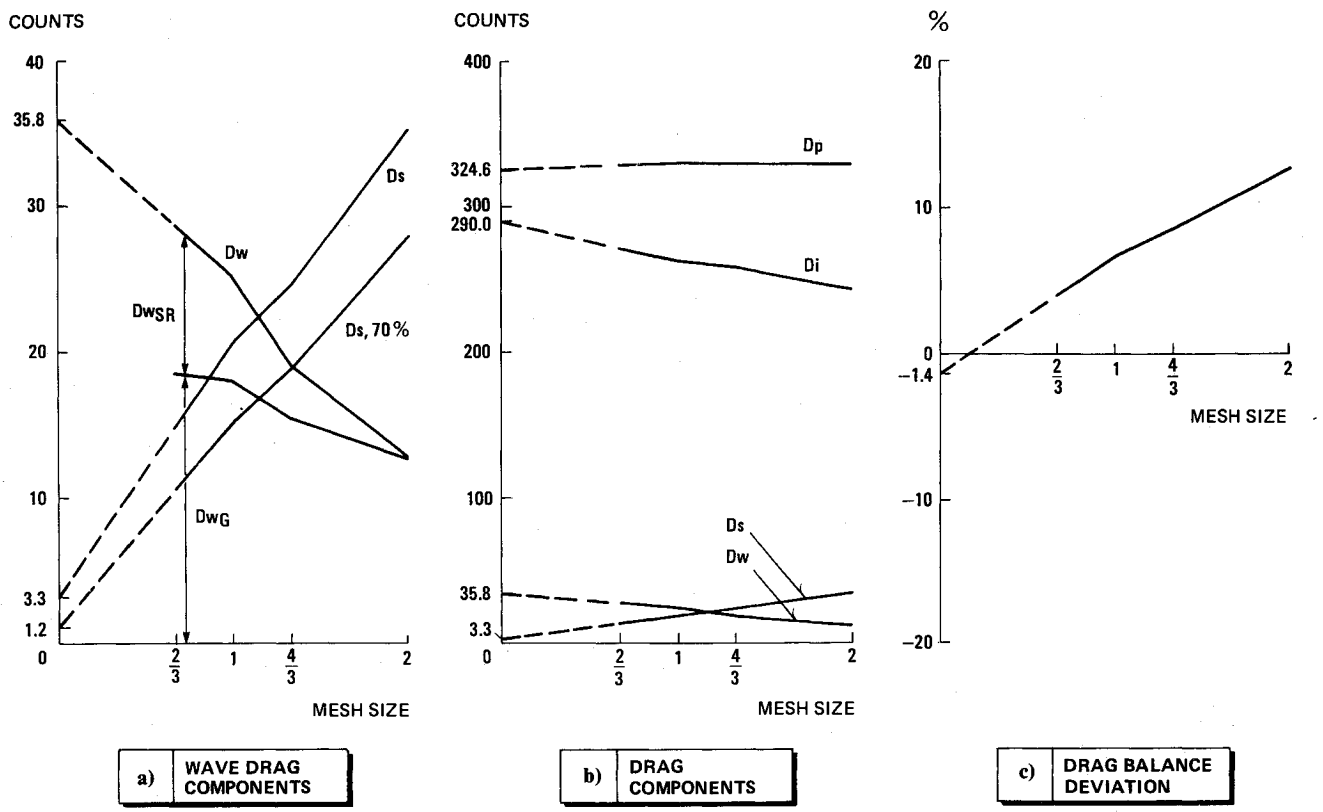

Fig. 3 Mesh refinement experiment, sequence CH.

CH-Topology Grid

A sequence of nested grids was used, as shown in Table 1. This sequence was generated using the grid generator MATGRID,[10] which was developed by FFA, Sweden, in the framework of the cooperative development of MATRICS and MATGRID. The ratio between the successive mesh sizes is approximately 2 : (4/3) : 1 : (2/3) in the vicinity of the wing. Because of restrictions on the grid dimensions stemming from the multigrid process in MATRICS and the central memory size of the computer, it was not possible to produce the previous mesh ratios exactly. All grids have the same global outer dimensions for the computational domain.

The results are plotted in Figs. 3a–3c. Figure 3a shows the three drag components related to the formation of shock waves. These are the Garabedian drag Dw_G, the shock remainder drag Dw_{SR}, and the spurious Garabedian drag $Dw_{G,spur}$. Note that the Garabedian drag and the shock remainder drag together determine the wave drag [compare with Eq. (18)]. The figure also shows the drag component Ds, 70%, which is the contribution to the spurious (Garabedian) drag on the inner 70% of the wing semispan. It can be observed that the spurious drag Ds indeed decreases about linearly with the mesh size, in agreement with theory. Consequently, its limit value for vanishing mesh size was determined by linear extrapolation from the results of the two finest grids. The limit value for Ds thus obtained is 3.3 counts. The fact that this value is not really close to the theoretical value zero seems to be mainly caused by the fact that the limit of vanishing mesh size cannot really be approached computationally on CH-topology grids. The reason is that the flow at the (cutoff) wing tip behaves singular in the spanwise coordinate, whereas the shape of the grid cells at the wing tip deteriorates under spanwise mesh refinement. As a consequence of this, the pressure distribution close to the wing tip (say, beyond 80% semispan[11,12]) is very sensitive to the spanwise mesh size. The previous reasoning is indeed substantiated by looking at the curve for Ds, 70%, which by a similar process of linear extrapolation leads to a limit value for vanishing mesh size of only 1.2 counts. In fact, the slope of this curve requires only a minor adjustment to actually attain the theoretical value zero. The limit value obtained for the wave drag as determined by linear extrapolation from the results of the two finest grids is $Dw = 35.8$ counts.

Figure 3b shows all drag components that enter the theoretical drag balance, Eq. (17). The limit values for the pressure drag and the induced drag as estimated by linear extrapolation are, respectively, $Dp = 324.6$ counts and $Di = 290.0$ counts.

Figure 3c finally shows the drag balance deviation defined as

$$\left(\frac{Dp}{Di + Dw + Ds} - 1\right) 100\% \tag{20}$$

Here the limit value for vanishing mesh size is obtained by substituting the limit values of each individual drag component in Eq. (20). The fact that this limit is only -1.4% seems to support the validity of the linear extrapolation used to determine limit values of drag components other than the spurious drag Ds.

CO-Topology Grid

CO-topology grids are boundary conforming to the rounded-off wing tip, Fig. 4. Compared with CH-topology grids, this implies a significantly higher and better balanced grid resolution in the vicinity of the wing tip. As a consequence, the tip vortex manifests itself much more clearly, and this can easily lead to such high induced velocities that the density can no longer be evaluated. This phenomenon will be referred to as expansion "beyond vacuum." This difficulty arises more easily with increasing freestream Mach number M_∞. It certainly did arise for the DFVLR-F4-wing at $M_\infty = 0.75$, $\alpha = 0.84$ deg, but it also occurred (though to a lesser extent) at low values of M_∞ where the flow is effectively incompressible. Note that this difficulty is not a prerogative of CO-topology grids. It has also been observed on CH-topology grids with increased resolution in the spanwise and/or the

wing-normal direction. The evidence therefore suggests that this difficulty is inherent to the calculation of transonic flow about wing tips on the basis of full-potential theory but only manifests itself if the grid around the wing tip is sufficiently fine to allow the computational development of the tip vortex.

Expansion beyond vacuum can be prevented in computations by modifying Eq. (2) to

$$\rho = \rho_0 = \{1 + [(\gamma - 1)/2]\, M_\infty^2 (1 - q_0^2)\}^{1/(\gamma - 1)} \tag{21}$$

as soon as

$$q^2 \geq q_0^2, \qquad q_0^2 < 1 + \frac{2}{(\gamma - 1)\, M_\infty^2} \tag{22}$$

Note that in regions where Eq. (22) is satisfied, the flow is assumed to be incompressible. A consistent way to calculate the pressure in those regions is then obviously to use Bernoulli's law.

The preceding modified flow model has been implemented in MATRICS by putting $q_0 = q_\infty$ and limiting the modification to a small subregion of the grid surrounding the wing tip and the entire edge of the assumed vortex sheet (Fig. 4). This choice forces the flow to be subsonic inside the subregion, allowing the correct treatment of stagnation, but avoiding shock waves and sonic surfaces. The reason for this particular choice has been mainly that the combination of the modified flow model and mixed supersonic/subsonic flow near the core of the tip vortex considerably slowed down the convergence speed of the multigrid algorithm in MATRICS and occasionally even led to limit cycle-type behavior after an error reduction between one and two orders of magnitude.

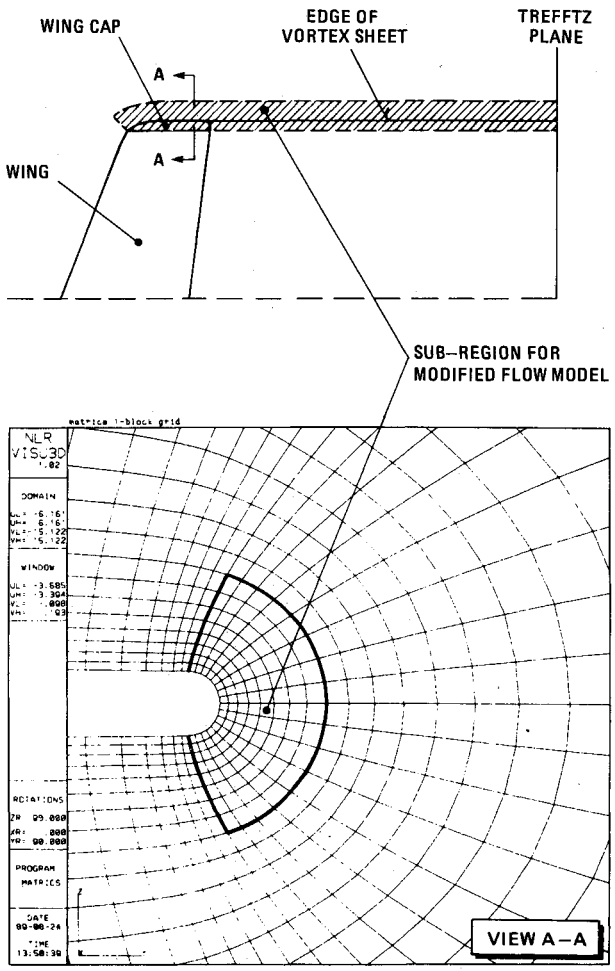

Fig. 4 Subregion for modified flow model with CO-topology grids.

A sequence of nested CO-topology grids was used, as shown in Table 1. All grids were generated using MATGRID. The ratio between the successive mesh sizes is again 2 : (4/3) : 1 : (2/3) (but this time not approximately and not only in the vicinity of the wing). All grids have the same outer dimensions for the computational domain.

The results are plotted in Figs. 5a–5c. Similarly as with the CH-sequence, Fig. 5a shows the three drag components Dw_G, Dw_{SR}, and Ds related to the formation of shock waves. Again, also the drag component Ds, 70%, which is the contribution to the spurious drag on the inner 70% of the wing semispan, is shown. It can be observed that the spurious drag Ds indeed decreases almost exactly linear with the mesh size as theory predicts. Consequently, all limit values were determined by linear extrapolation to vanishing mesh size from the results of the two finest grids. The limit value for Ds is 4.4 counts, which is again not really close to the theoretical value zero. Similarly, as with CH-topology grids, the limit value for Ds, 70%, is much lower, namely 1.7 counts, and this indicates that the main cause of why the limit value for Ds deviates more from zero than expected is to be found in the wing tip region. Since there is no reason why the modified flow model should not converge in the mesh size, the only explanation left open is that the tip vortex is not sufficiently resolved on the grid, despite the 24 almost square cells around the wing cap on the finest grid of the sequence (compare Fig. 4 where there are 16 cells around the wing cap). It is therefore a bit questionable whether the extrapolated curve for the pressure drag Dp predicts an accurate limit value (327.6 counts). The curves for the induced drag Di (Fig. 5b) and the wave drag Dw (Fig. 5a) can be seen to behave quite normally and lead to limit values of 289.1 and 40.3 counts, respectively. With respect to the pressure drag, it is indicative to observe the following. If the wing cap (Fig. 4) is dropped in the surface integration leading to the pressure drag, the need for extremely high resolution is confined to the immediate vicinity of the core of the tip vortex inside the subregion where the modified flow model is effective. It is then possible to devise a correction procedure to determine the pressure drag more accurately. Assume a perfect drag balance in the limit of vanishing mesh size. This leads to a corrected limit value for the pressure drag Dp, viz.,

$$(Dp)_{\text{limit}} = (Di + Dw + Ds)_{\text{limit}}$$

$$= 289.1 + 40.3 + 4.4 = 333.9 \text{ counts} \tag{23}$$

Subsequently, determine the limit value of the pressure drag while neglecting the wing cap,

$$(Dp,\text{wing})_{\text{limit}} = 325.5 \text{ counts} \tag{24}$$

It follows that the contribution of the wing cap to the pressure drag is

$$(Dp,\text{wing cap})_{\text{limit}} = (Dp - Dp,\text{wing})_{\text{limit}} = 8.3 \text{ counts} \tag{25}$$

Finally, the corrected pressure drag is calculated as

$$Dp = Dp,\text{wing} + (Dp,\text{wing cap})_{\text{limit}}$$

$$= Dp,\text{wing} + 8.3 \text{ counts} \tag{26}$$

The resulting values and the corresponding drag balance deviations are plotted in Figs. 5b and 5c. It can be observed that the corrected pressure drag is hardly affected by mesh size variations (deviations from the limit value are within about 0.5%), whereas the drag balance deviation is within 4%. With respect to the induced drag, it can be remarked that even on the coarsest grid in the sequence (relative mesh size 2) the calculated value is only 3.7% below the limit value, and this clearly demonstrates the advantage of CO-topology grids over CH-topology grids in calculating induced drag. With respect

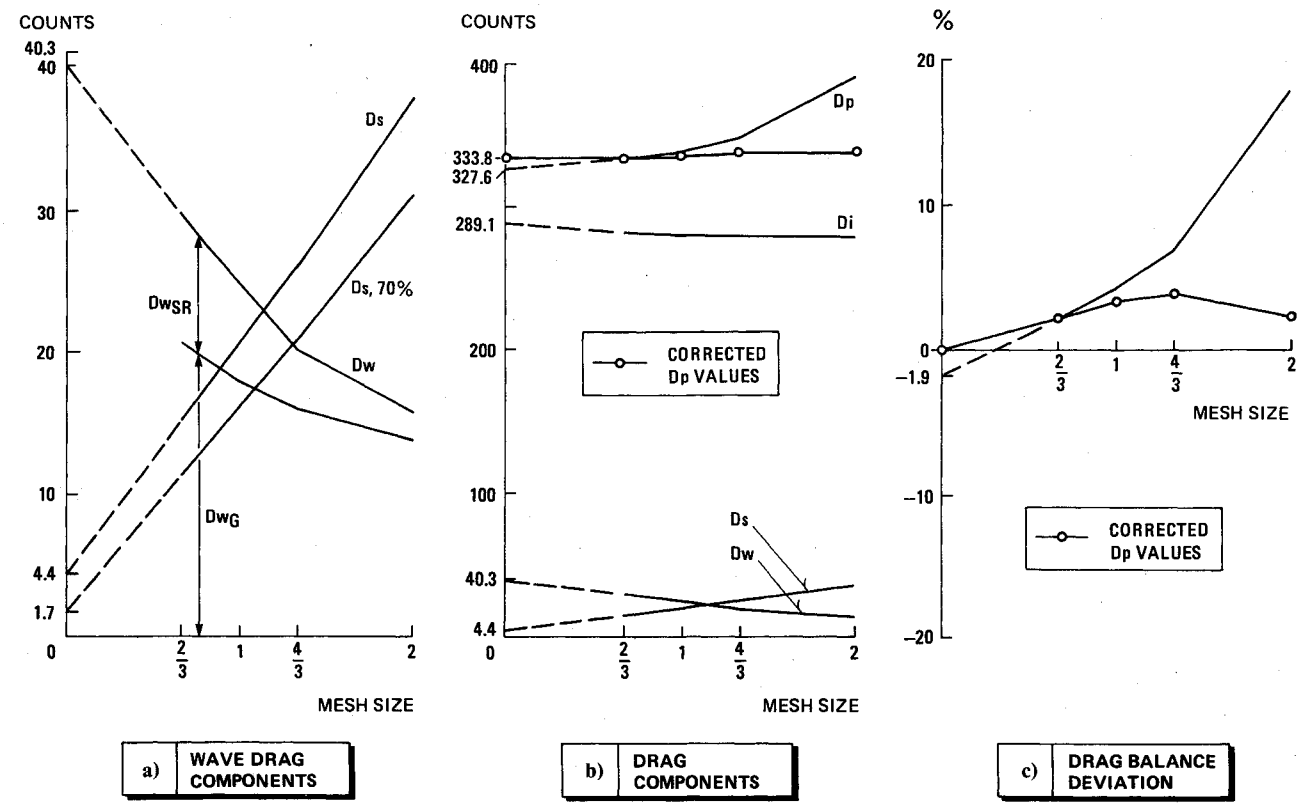

Fig. 5 Mesh refinement experiment, sequence CO.

to the wave drag, the situation is apparently similar to that on CH-topology grids, because even on the finest grid in the sequence (relative mesh size 2/3 with 552,960 mesh cells) the wave drag is still 26% below its limit value.

V. Conclusions

With the purpose of providing insight into the inviscid drag prediction for transonic transport wings using a full-potential method, mesh refinement experiments have been carried out on both CH- and CO-topology grids. An important aspect has been to investigate linear extrapolation to the limit of vanishing mesh size as a means of calculating reliable values for the various components in the drag balance for the transonic regime and also to economize on computational costs.

With respect to CH-topology grids, mesh refinement experiments indicate that linear extrapolation to vanishing mesh size on the basis of results on two sufficiently fine nested grids leads to an acceptably satisfied drag balance. This fact suggests improved accuracy of each individual drag component. This is supported by the following two observations. First, the induced drag can be seen to depend heavily on the mesh size. Second, the wave drag depends even more heavily on the mesh size. However, because the limit of vanishing mesh size cannot really be reached computationally on CH-topology grids due to deterioration of the grid at the wing tip, there probably always remains room for some arbitrariness in the drag obtained in purely inviscid potential flow on CH-topology grids.

With respect to CO-topology grids, the mesh refinement experiments have first of all clearly exposed the difficulty that the flow tends to expand beyond vacuum in the core of the tip vortex. This difficulty becomes more serious as the grid resolves the tip vortex better, which by itself has turned out to be a requirement for good results in doing a lift/drag analysis. The difficulty could be avoided by introducing a modified flow model that locally solves for incompressible flow if the velocity gets higher than a prescribed subsonic value (in all experiments the freestream velocity has been taken). Next, mesh refinement has shown that sufficient grid resolution for the tip vortex is essential to obtain a meaningful contribution of the rounded-off wing tip to the surface-integrated pressure drag. In fact, this resolution should be at least as good as with the (finer) grids in the sequence CO (Table 1). However, the values obtained for the induced drag on the various grids did not depend much on the wing tip resolution and in general on the relative mesh size of each particular grid. Apparently, the circulation close to the rounded-off wing tip depends less critically on the local grid resolution. Both on CH- and CO-topology grids, the wave drag depends heavily on the mesh size and can be as much as 20–26% too low as compared with its limit value on the finest grids in each sequence. This is probably mainly a consequence of the first-order accuracy of the MATRICS finite-volume scheme throughout supersonic flow regions.

The aforementioned observations lead to two cautious conclusions. First, CO-topology grids are better suited for drag analysis than CH-topology grids. Second, for the transonic flow regime, linear extrapolation to the limit of vanishing mesh size improves the accuracy of each individual drag component, in particular that of the wave drag.

On the basis of the experiments carried out, it is finally conjectured that accurate calculation of the various drag components directly on one grid would require between 10^7 and 10^8 grid points using first-order-accurate finite-volume schemes throughout supersonic flow regions, which is impossible on even today's biggest supercomputer. This stresses the need for artificial viscosity terms that are second-order small in the mesh size in supersonic flow regions, except for the immediate vicinity of the shock waves (see, e.g., Ref. 13). Then it can be expected that the number of grid points required for accurate drag prediction with viscous/inviscid full-potential interaction codes can be kept on a much more reasonable level. However, it is believed that extrapolation procedures like the one discussed in the present paper still remain necessary in an engineering environment.

Acknowledgment

This investigation has been carried out partly under a contract awarded by The Netherlands Agency for Aerospace Programs (NIVR), Contract RB 311.1-0150 N. The authors wish to express their thanks to their colleague Fennanda Doctor for her endeavors in preparing most of the grids.

References

[1]Van der Vooren, J., and van der Wees, A. J., "Inviscid Drag Prediction for Transonic Transport Wings Using a Full-Potential Method," AIAA Paper 90-0576, Jan. 1990; also NLR TR 89365 U, 1989.

[2]Chow, R., "Solution of Viscous Transonic Flow over Wings," *Computers and Fluids,* Vol. 13, No. 3, 1987, pp. 287–317.

[3]Van der Vooren, J., van der Wees, A. J., and Meelker, J. H., "MATRICS, Transonic Potential Flow Calculations about Transport Aircraft," *AGARD Conference Proceedings,* No. 412, 1986.

[4]Van der Wees, A. J., "FAS Multigrid Employing ILU-SIP Smoothing: A Robust Fast Solver for 3D Transonic Potential Flow," *Multigrid Methods II. Proceedings of the 2nd European Conference on Multigrid Methods,* edited by W. Hackbush and U. Trottenberg, Lecture Notes in Mathematics 1228, Springer-Verlag, Berlin, 1986, pp. 399–416.

[5]Van der Vooren, J., "Aircraft Drag Prediction for Transonic Potential Flow," *Technical Status Review on Drag Prediction and Analysis from Computational Fluid Dynamics: State of the Art,* AGARD Advisory Rept. 256, Paper 5, June 1989; also NLR MP 88022 U, 1988.

[6]Garabedian, P. R., "Computation of Wave Drag for Transonic Flow," *Journal d'Analyse Mathématique,* Vol. 30, 1976, pp. 164–171.

[7]Garabedian, P. R., and McFadden, G., "Computational Fluid Dynamics of Airfoils and Wings," *Proceedings of Symposium on Transonic Shock and Multidimensional Flows,* Academic Press, New York, 1982, pp. 1–16.

[8]Garabedian, P. R., and McFadden, G., "Design of Supercritical Swept Wings," *AIAA Journal,* Vol. 20, No. 3, March 1982, pp. 289–291; also AIAA Paper 82-4058, 1982.

[9]Ross, D. S., "Redesign of a Supercritical Wing in the Presence of an Engine Nacelle," *Journal of Computational Physics,* Vol. 73, 1987, pp. 233–243.

[10]Tysell, L. G., and Hedman, S. G., "Towards a General Three-Dimensional Grid Generation System," International Council of the Aeronautical Sciences, ICAS-88-4.7.4, Jerusalem, Israel, 1988.

[11]Carr, M. P., "Accuracy Study of Transonic Flow Computations for 3-D Wings," AGARD 62nd FDP Symposium on Validation of Computational Fluid Dynamics, Paper 18, Lisbon, Portugal, May 1988.

[12]"Accuracy Study of Transonic Flow Computations for Three Dimensional Wings," Vol. 1—Text, Vol. 2—Tables and Figures, GARTEUR Action Group AD, TP-030, March 1988.

[13]Rubbert, P. E., et al., "A New Approach to the Solution of Boundary Value Problems Involving Complex Configurations," American Society of Mechanical Engineers, ASME Winter Annual Meeting, Anaheim, CA, Dec. 1986; also *Computational Mechanics—Advances and Trends—AMD,* edited by A. K. Noor, Vol. 75, Book H00344.